Journal of Power Sources 214 (2012) 200–207

Contents lists available at SciVerse ScienceDirect

Journal of Power Sources

journal homepage: www.elsevier.com/locate/jpowsour

Non-aqueous electrodeposition of porous tin-based film as an anode for lithium-ion battery

C.D. Gu*, Y.J. Mai, J.P. Zhou, Y.H. You, J.P. Tu

State Key Laboratory of Silicon Materials and Department of Materials Science and Engineering, Zhejiang University, Hangzhou 310027, China

HIGHLIGHTS

- Porous tin-based film with double-layer structure, i.e. SnO_2/Sn–Cu.
- Tin-based film electrodeposited from Ethaline based electrolyte.
- Self-assembly distribution constructing an open and bicontinuous porous Sn network.
- Double-layer tin-based film delivering a satisfactory Li ion storage capacity.

GRAPHICAL ABSTRACT

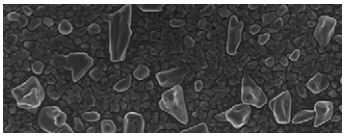

ARTICLE INFO

Article history:
Received 9 December 2011
Received in revised form
23 February 2012
Accepted 26 April 2012
Available online 6 May 2012

Keywords:
Ionic liquid
Electrodeposition
Tin
Lithium-ion batteries

ABSTRACT

Porous tin-based films are electrodeposited on copper foils from a choline chloride/ethylene glycol based electrolyte containing $SnCl_2 \cdot 2H_2O$ without any complexing agent or additive. Increasing the deposition time and voltage produces thicker films. The initially deposited Sn grains are relatively uniform with an average size of 200–300 nm and a kind of self-assembly distribution constructing an open and bicontinuous porous network. The architecture of these films possesses a double-layer structure, i.e. SnO_2 (superficial layer)/Sn–Cu alloy (bottom layer), which is revealed by X-ray diffractometer and X-ray photoelectron spectroscopy. The electrochemical performance of the porous tin-based films as anode for lithium-ion batteries is measured. Although the capacity fades gradually with repeated cycling, a reversible capacity of 300-350 mAh g^{-1} is maintained for more than 50 cycles, which suggests that the in situ formed Sn–Cu alloy could provide an interlocking interface between active materials and current collector. Therefore, the tin's shedding from the current collector can be restrained. Moreover, the inactive materials, such as the oxide in the superficial layer and the Cu in the bottom layer, could also act as buffers to relieve the induced volume expansion of Sn during the repeated lithiathion/delithiation process, thus giving the good cycle performances.

1. Introduction

As for the current commercial rechargeable lithium-ion batteries, carbonaceous materials are the most commonly used anode materials due to their low cost and low electrochemical potentials with respect to lithium metal [1–3]. However, since their theoretical capacity is only 372 mAh g^{-1}, there are demands to develop new anode materials with higher capacity to enhance the energy density of lithium-ion batteries as a power supply for portable electric devices and electric vehicles. Tin-based materials have been focused on because their capacity (994 mAh g^{-1}, the theoretical limit of $Li_{4.4}Sn$) largely exceeds that of graphite [4–6]. However, severe volume expansion in the pure tin anode would occur due to lithiation/delithiation process during charge-discharge cycles, which causes poor cycle performance and inhibits its application in lithium-ion batteries [7,8]. Therefore, tin

* Corresponding author. Tel./fax: +86 571 87952573.
E-mail addresses: changdong_gu@hotmail.com, cdgu@zju.edu.cn (C.D. Gu).

0378-7753/$ – see front matter © 2012 Elsevier B.V. All rights reserved.
doi:10.1016/j.jpowsour.2012.04.085

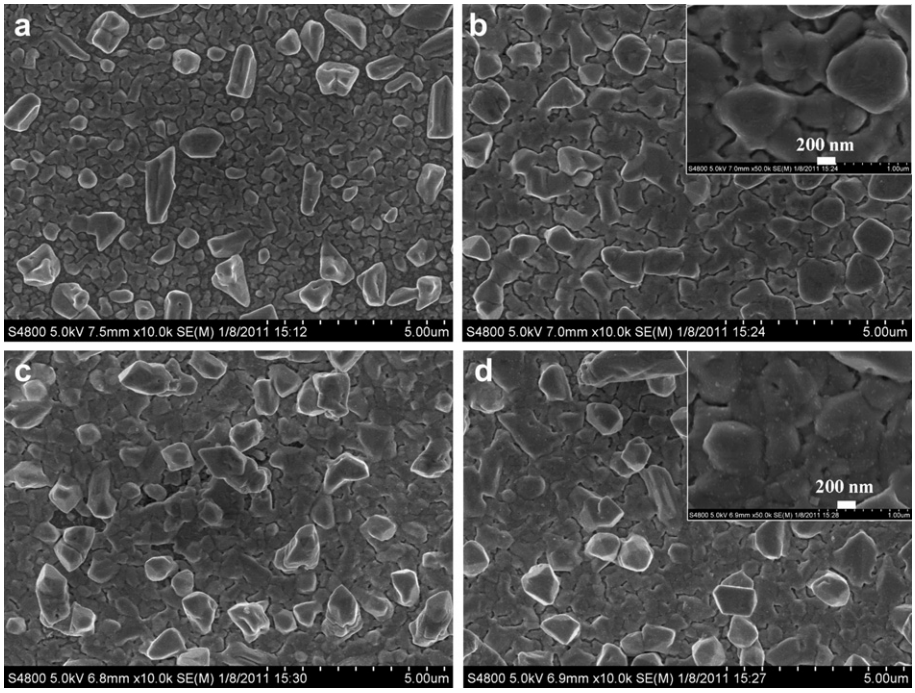

Fig. 1. Surface morphologies of as-deposited Sn-based films at 0.5 V for different deposition time. (a) 2 min; (b) 5 min; (c) 10 min; (d) 15 min. Insets are the corresponding magnified SEM pictures.

oxides [9–14] or tin-based alloys (for example, Sn–Zn [15], Sn–Sb [16,17], Sn–Co [18], and Sn–Cu [5,19–21]) have been attracted much more attentions due to their better cyclability than pure tin because of the inactive elements in the oxides or alloy buffer volume changes during charge/discharge cycling.

In order to enhance the cyclability of tin-based active materials, a good electronic conductivity among the active materials and at the interface between them and the current collector is desirable [5]. Electrodeposition is a versatile bottom-up processing method that can be used to deposit metals, ceramics, polymers, and semiconductors in a wide range of microstructures and nanostructures. The method is inexpensive and relatively simple, and especially it can support a good interface strength and electronic conductivity between the coating metals and the substrate. The electrodeposited Cu_6Sn_5 film is one of the most promising anode materials because of its low price, high conductivity, and good retention of capacity [5,19,20]. However, the usual procedure of Sn or Sn-based alloys electrodeposition is mostly based on aqueous solutions of which there are limitations including the poisonous plating baths, the necessity for complexing agents and additives, and the difficult handling of hydrogen evolution processes [5,19,20]. Room-temperature ionic liquids are more advantageous green solvents for the electrodeposition of metals due to their wide electrochemical windows, extremely low vapour pressures, and numerous, only partly understood, cation/anion effects [22–24]. Sn or Sn-based alloys have been successfully electrodeposited from ionic liquids [25–29]. Moreover, the macroporous Sn was direct electrodeposited from a water- and air-stable room-temperature ionic liquid, namely, 1-ethyl-3-methylimidazolium-dicyanamide [26]. The porous Sn or Sn-based alloy would be a good anode candidate for the lithium-ion batteries because the porous structure could relieve the anode of the severe volume expansion in the lithiation/delithiation process.

Recently, we have demonstrated that nanoporous Ag films on copper alloy substrates could be fabricated by the galvanic replacement reaction from the mixture (1:2 mol ratio) of choline chloride/ethylene glycol (Ethaline) containing AgCl [30]. It was suggested that the viscous Ethaline might be the soft template for the formation of nanoporous Ag deposits [30]. Ethaline, one of typical deep eutectic solvents with non-aggressive nature invented by Abbott and co-workers [31] is a promising solvent used for the deposition of a range of metal films, for example, Zn, Sn, and Cu, at high current efficiency [28,32,33]. However, the electrodeposition of porous Sn-based films from the non-aggressive ethaline have not been explored. Based on this thought, this paper investigates the facile electrodeposition of porous Sn films from the Ethaline based electrolyte and their microstructure and lithium storage performance. Importantly, it is found that the composition of the as-deposited Sn films is SnO_2/Sn–Cu alloy double-layer structure exhibiting a good electrochemical performance during the cycled lithiation/delithiation process.

2. Experimental

2.1. Electrodeposition and characterization of the porous tin-based anode

Choline chloride (AR, Aladdin) and ethylene glycol (AR, Aladdin) were used as received. The homogeneous colorless Ethaline was formed by stirring the mixture of the two components in a mol ratio of 1 choline chloride : 2 ethylene glycol at 80 °C for about 30 min. The electrolyte is the Ethaline solution containing 0.1 M $SnCl_2 \cdot 2H_2O$. The substrate was the copper foil with a thickness of about 0.03 mm, which was served as the current collector for the anode in lithium-ion batteries. A surface cleaning treatment of the substrate was conducted to remove the industrial oil by electrolytic degreasing and deionized water rinsing. Before the electroplating process, the substrate was dried with flowing air. The porous tin-based film was direct-current electroplated from the above electrolyte bath at variable applied voltages and ambient temperature (25 ± 3 °C) without the deaeration process. During the electrodeposition process, the anode consisted in a tin plate. The final

deposits were sequentially rinsed with methanol and deionized water.

A field emission scanning electron microscope (FE-SEM, Hitachi S-4800) was employed for the observations of the film surface and an energy dispersive X-ray spectrometer (EDS) attached was used for qualitative elemental chemical analysis. Crystalline structure of the deposits was studied by X-ray diffractometer (XRD, Rigaku D/max 2550PC, Japan) with a Cu target ($\lambda = 1.54056$ Å) and a monochronmator at 40 kV and 250 mA with the scanning rate and step being 4° min^{-1} and 0.02°, respectively. X-ray photoelectron spectroscopy (XPS, AXIS UTLTRADLD) was used to characterize the composition and chemical state of the product using Al (monochromatic) Kα radiation with $E = 1486.6$ eV. All core-level spectra were referenced to the C 1 s peak at 284.8 eV assumed to originate from the surface hydrocarbon contamination. The composition depth profile of the film was analyzed by combining a sequence of ion gun etch cycles (etching rate ~5–6 nm min^{-1}) interleaved with XPS measurements.

2.2. Electrochemical measurements of the porous tin-based anode

Electrochemical performances of the electrodeposited tin-based anodes were investigated with two-electrode coin-type cells (CR 2025) assembled in an argon-filled glove box with the metallic lithium foil as both the reference and counter electrodes, 1 M $LiPF_6$ in ethylene carbonate (EC)-dimethyl carbonate (DME) (1:1 in volume) as the electrolyte, and a polypropylene (PP) micro-porous film (Cellgard 2300) as the separator. Charge-discharge tests were conducted on LAND battery program-control test system between 0.05 and 3.0 V at a rate of 100 mA g^{-1}. Cyclic voltammetry (CV) was performed on CHI660C electrochemical workstation in the potential ranges of 0.02–3.0 V at a scan rate of 0.1 mV s^{-1}.

3. Results and discussion

3.1. Surface morphology

Fig. 1 gives the deposition time-dependent surface morphologies of the electrodeposited Sn films from the Ethaline based electrolyte at 0.5 V. After 2 min deposition, the substrate was covered by the netlike Sn deposits as shown in Fig. 1a. It is found that the initially deposited Sn grains are relatively uniform with an average size of 200–300 nm and a kind of self-assembly distribution. The connected Sn grains construct an open and bicontinuous porous network between them with the pore size in the range of 30–40 nm. It is also found that a few larger Sn grains with the size of about 1 μm are randomly distributed in the Sn network, which may be due to the preferential growth of deposits in the current convergence area of the substrate. When prolonging the deposition time to 5 min, the size of netlike Sn grains increase to about 500–700 nm, as shown in Fig. 1b. However, the pores between grains still exist and retain the size of about 20–30 nm. At the deposition times of 10 and 15 min, grains are ready to connect each other at the expense of pores as shown in Fig. 1c and d. It can be seen that at 0.5 V with increasing the deposition time, the film density is accordingly increased. However, pores still exist in the film obtained from the Ethaline based electrolyte, which is largely different from the Sn-based film electrodeposited from the aqueous electrolyte with a dense microstructure [19,20]. Fig. 2 gives the surface morphologies of the electrodeposited Sn films from the Ethaline based electrolyte at 0.7 V for 5 (a) and 15 min (b), respectively. After 5 min deposition, the Sn film obtained at 0.7 V has a similar surface morphology with those obtained at 0.5 V (see Fig. 1). However, with prolonging the deposition time to 15 min, a rougher surface is obtained at 0.7 V, where plenty of cone-like Sn

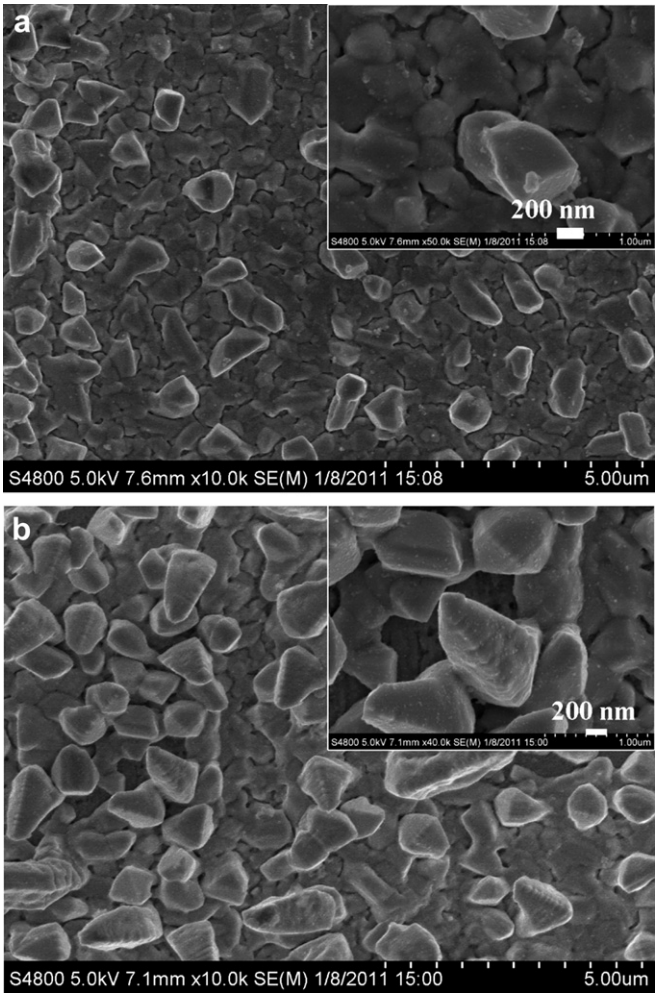

Fig. 2. Surface morphologies of as-deposited Sn-based films at 0.7 V for (a) 5 min and (b) 15 min, respectively. Insets are the corresponding magnified SEM pictures.

grains with the size of about 1 μm randomly grow on the surface leaving much more pores in the films.

Fig. 3a and d give typical cross-section morphologies of the electrodeposited Sn films at 0.7 V for 5 min and for 15 min, respectively, from which it can be seen that the Sn films are tightly adhered to the brass substrate. With the EDS mapping analysis of elements Sn (such as Fig. 3b and e) and Cu (such as Fig. 3c and f), the thickness values of the electrodeposited films can be roughly determined and are summarized in Table 1. It is indicated that increasing the deposition time and voltage would produce thicker films. However, the film thickness seems not to be uniform, which should be related to the porous structure of the films.

3.2. Crystal structure and composition

Fig. 4 gives the typical XRD patterns of the electrodeposited Sn films on the copper substrate at 0.5 V and 0.7 V, respectively. In Fig. 4, the peaks at 43.3°, 50.4°, and 74.1° are assigned to the face-centered cubic (fcc) Cu substrate planes of (111), (200), and (220), respectively. The other peaks should be attributed to the Sn films, which indicates the presence of two basic phases in both Sn films shown in Fig. 4: the β-Sn (JCPDS 04-0673) and Cu_6Sn_5 (JCPDS 02-0713). The weak peak at 30.2° is assigned to (101) plane of Cu_6Sn_5 phase. The *in situ* formation of Cu_6Sn_5 layer can be attributed to the mutual diffusion of the Sn and Cu atoms. Du et al. also found that

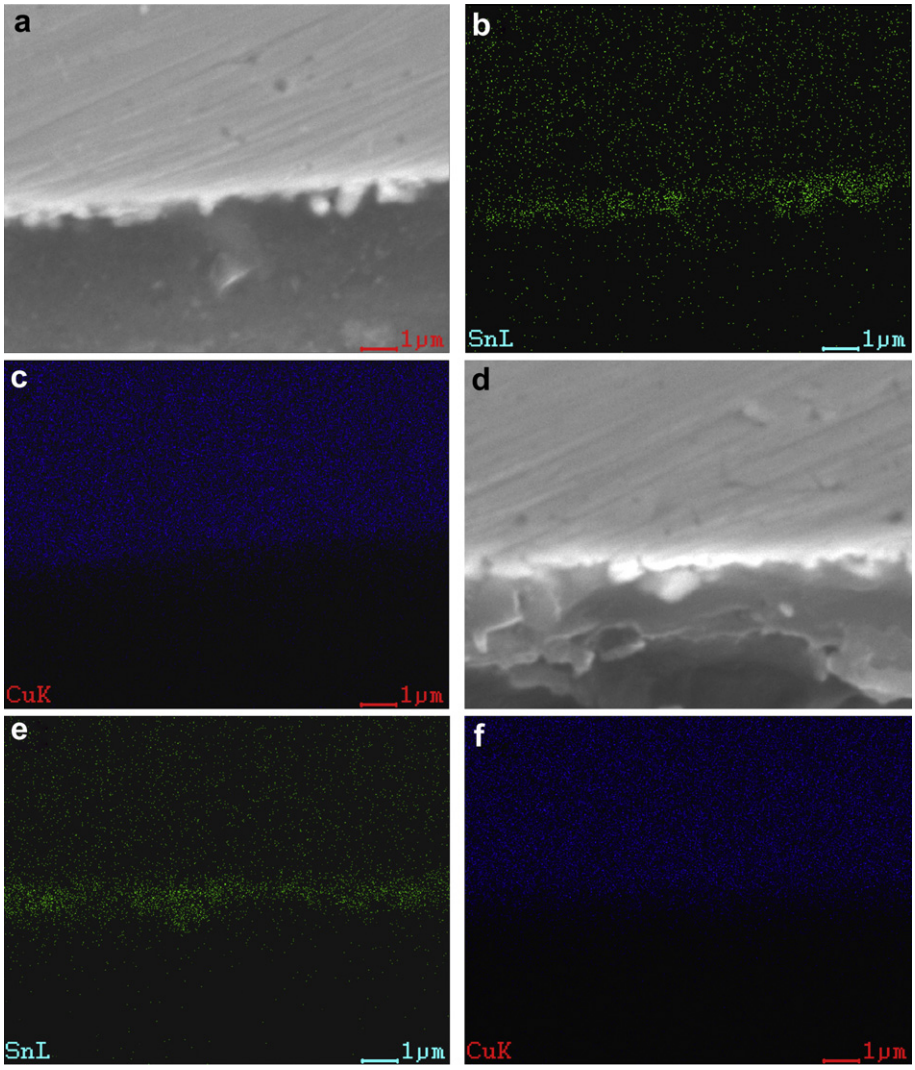

Fig. 3. Typical cross-section morphology and EDS mapping analysis of the electrodeposited Sn-based films at 0.7 V for 5 min (a, b, and c) and at 0.7 V for 15 min (d, e, and f).

the Cu_6Sn_5 layer was formed in the electroless plating Sn on the copper foam [20]. The study of Tamura et al. indicated the electrodeposition process of tin on copper without heat treatments could form a slight Cu_6Sn_5 intermetallic compound layer at the interface between tin and copper [5]. As for the lithium batteries, the formation of Cu_6Sn_5 layer could enhance the bonding force between active materials and current collector, which restrains tin's shedding from the current collector and leads to good cycling performance [5,20].

The XPS analysis is carried out to investigate the surface structure of the Sn film as shown in Fig. 2, and the corresponding results are shown in Fig. 5. The binding energies in the XPS spectra are calibrated by using that of C 1 s (284.8 eV). All peaks in the XPS full spectrum shown in Fig. 5a can be ascribed to Sn, C, and O elements. The presence of C comes mainly from pump oil in the vacuum system of the XPS equipment. The presence of O implies that tin oxide layer should be formed on the film's surface. The high-resolution spectra for Sn is shown in Fig. 5b, where the two main peaks centered at 486.2 and 494.7 eV can be assigned to Sn $2d_{5/2}$ and Sn $3d_{3/2}$ for SnO_2, respectively. There are two small satellite peaks can be found at 484 and 492.5 eV, respectively, which might be assigned to the pure Sn. The XPS result of Fig. 5b indicates that small amount of SnO_2 forms the top surface layer of the electrodeposited Sn films. The architectures of the electrodeposited Sn films are further illustrated by the XPS composition depth profile as shown in Fig. 5c and d. The atomic concentrations of Cu, O, Sn and C as the main elements in the films show variations throughout the film thickness. As shown in Fig. 5c for the film obtained at 0.7 V for 5 min, the atomic concentration ratio of O/Sn is nearly 2 at the first 60 s of sputter time, which should be responsible for the thin SnO_2 layer on the film surface. However, the concentration of O rapidly decreases to about 0 after about 180 s of etching. Accordingly, the Sn concentration increases to the maximum value at the sputter time of 120 s. Then, the concentration of Sn decreases gradually accompanied with the gradually increasing of the atomic concentration of Cu, which should correspond to the Cu_6Sn_5 transition layer at the interface of the film and the substrate. Based on the result of XRD (Fig. 4) and XPS (Fig. 5c) measurements, it can be seen that the electrodeposited porous film possesses double-layer architecture, i.e. SnO_2/Sn–Cu alloy from the top layer to the bottom layer. For comparison, the XPS composition depth profile of the film obtained at 0.7 V for 15 min is presented in Fig. 5d, from which the double-layer structure of the porous Sn-based film is further proved. Moreover, after the same etching duration, the atomic concentration of Sn in the film still holds around 30%, which indicates that the double-layer film obtained at 0.7 V for 15 min is

Table 1
Thickness of electrodeposited Sn-based films determined by the EDS mapping analysis.

Deposition condition	Thickness/μm
At 0.5 V for 5 min	0.35 ± 0.1
At 0.5 V for 15 min	0.75 ± 0.2
At 0.7 V for 5 min	0.48 ± 0.1
At 0.7 V for 15 min	0.92 ± 0.2

much thicker than that obtained at 0.7 V for 5 min. Furthermore, in the double-layer film the thickness of bottom layer (Sn–Cu alloy) is much higher than that of the top layer (SnO_2). The Sn–Cu layer constructs the interlocking interface between the film and the substrate, which is believed to support good interface strength.

3.3. Electrochemical performance

The porous Sn-based films with double-layer architecture of SnO_2/Sn–Cu alloy are expected to deliver good electrochemical performances as potential anodes in lithium batteries due to their composite characteristic and porous structures. The typical lithium insertion/extraction profiles of the electrodeposited Sn-based film obtained at 0.7 V for 15 min at a current density of 100 mA g^{-1} are demonstrated in Fig. 6, in which the voltage window is fixed from 0.05 to 3.0 V. In the first discharging process, the potential drops rapidly to a small plateau of about 0.6 V, and then decreases gradually to a large plateau of about 0.4 V. Lastly, the potential further gradually decreases to the stop potential of ~0.05 V. The plateau around 0.6 V should correspond to the irreversible reaction of top SnO_2 layer with lithium to form Li_2O and Sn [11,34] and the formation of the solid electrolyte interface (SEI) layers [9,35], which almost disappears in the following cycles as shown in Fig. 6. The inactive Li_2O disperses in the top layer of the Sn-based film, which could relieve the volume changes during the following charge/discharge cycling. The plateau around 0.4 V should be attributed to the Li intercalation process of Sn and Cu_6Sn_5 compositions [5,36], which corresponds to the formation of Li_2CuSn phase and the end produce of the full lithiation of the Cu_6Sn_5 and Sn should be $Li_{4.4}Sn$

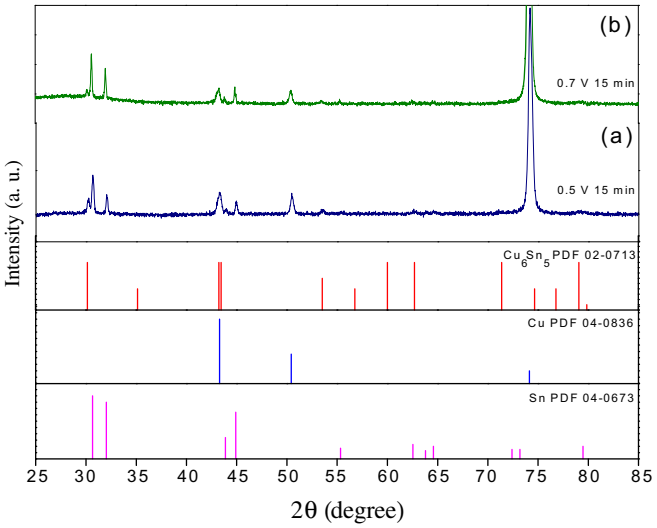

Fig. 4. XRD patterns of the electrodeposited Sn-based films on the copper substrate. (a) at 0.5 V for 15 min; (b) at 0.7 V for 15 min.

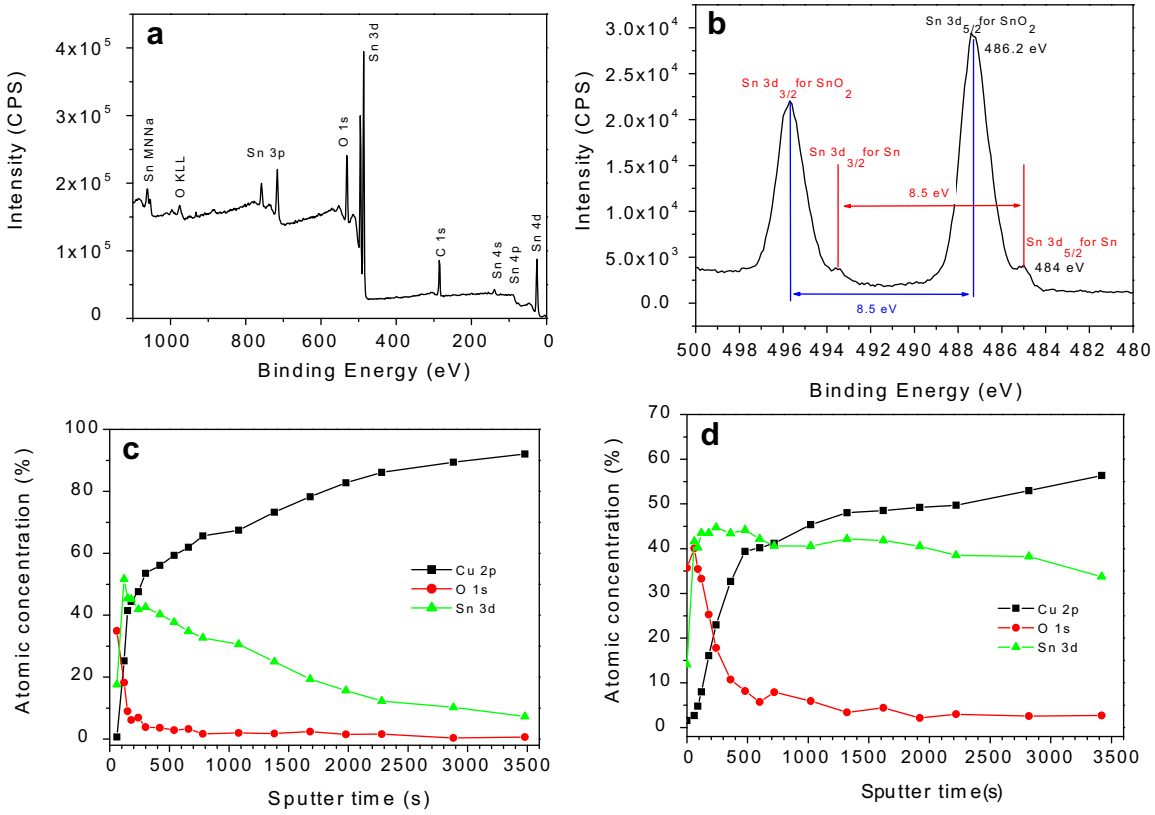

Fig. 5. (a) XPS full spectrum of the Sn-based film electrodeposited at 0.7 V for 5 min. (b) High-resolution spectra for Sn species. (c–d) XPS composition depth profiles from the Sn-based films (c: 0.7 V for 5 min; d: 0.7 V for 15 min).

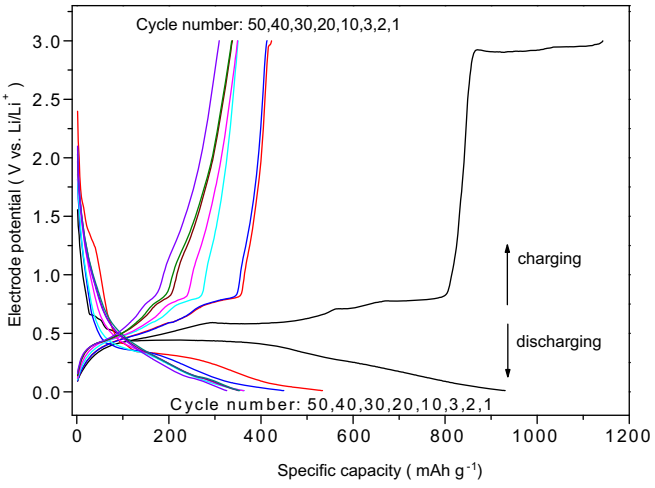

Fig. 6. Charge-discharge curves of the Sn-based anode electrodeposited at 0.7 V for 15 min. Electrode potential range: 0.05–3.0 V vs. Li/Li^+, charge-discharge current density: 100 mA g^{-1}.

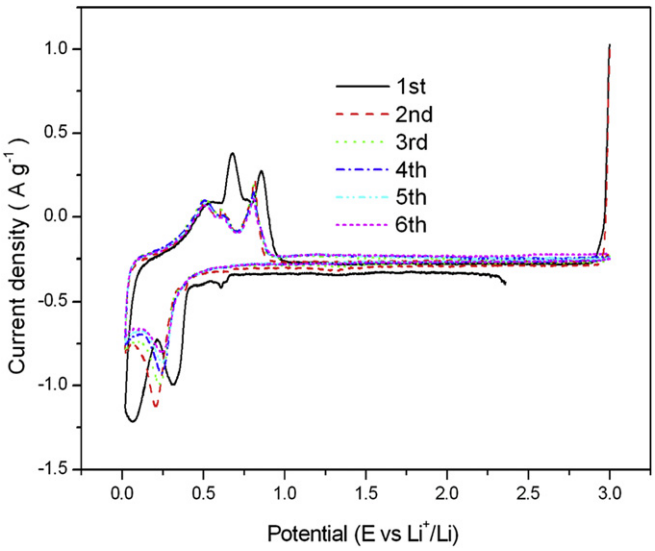

Fig. 7. CV curves for the electrodeposited Sn-based film obtained at 0.7 V for 15 min.

and Cu [36]. In the first charging process, the anode potential changes to about 0.4 V versus Li/Li^+ immediately after starting the test, stabilized, and then gradually changed toward the negative again. It is considered that the plateau results from the reformation of the Sn–Li intermetallic in a multistep reaction [36]. The further gradual increase of anode potential results from a coexistence with several Sn–Li alloy phases in the active material [5,36]. The 0.8 V plateau during the charge process of the Sn-based electrode should be associated with the coexistence of $Li_{2-x}CuSn$ and Cu_6Sn_5 [36]. The bottom layer of the porous Sn-based film, mainly the *in situ* formed Cu_6Sn_5 in this study, could enhance the bonding force between active materials and current collector and restrain tin's shedding from the current collector [5,20]. Moreover, the inactive Cu in the bottom layer would also act as buffers to relieve the induced volume expansion of Sn in the lithiation/delithiation process.

It is worth noting that the first charging process of the battery shown in Fig. 6 exhibits an abnormal plateau behavior when the anode potential changed to about 2.9 V versus Li/Li^+, which makes the coulombic efficiency of the first cycle above 100%. This phenomenon is observed for all the batteries of this study. The abnormal potential plateau around 2.9 V versus Li/Li^+ disappears in the following cycles as shown in Fig. 6. The 2.9 V plateau corresponds to the highest irreversible anode peak shown in the first cycle of CV curves (Fig. 7), which might be related to the presence of oxygen in the system or other unknown oxidation reactions. The disappearance of the 2.9 V potential plateau in the following cycles indicates that the remnants O might be exhausted or the formation of undecomposable oxides. In the following cycles, charge-discharge curves shown in Fig. 6 have the similar profile with good cyclability and efficiency.

The CV curves for the electrodeposited Sn-based film at 0.7 V for 15 min are given in Fig. 7. The irreversible reduction peak centered at ~0.6 V during the first cycle should be related to the formation of SEI layers and the irreversible reaction of top SnO_2 layer with lithium to form Li_2O and Sn as described above. The electrode shows reversible behavior from the second to the following cycles. The reduction waves ranging from 0.01 to 0.4 V correspond to the fully Li intercalation processes to form the $Li_{4.4}Sn$ and Cu [36]. The oxidation peaks from ~0.4 to ~0.8 V should be corresponding to the reformation of Cu_6Sn_5.

Fig. 8 displays the cycleability and coulombic efficiency curves of the electrodeposited Sn-based samples. Except for the abnormal first cycle, the sample of 0.7 V 15 min holds the highest coulombic efficiency of more than 96%. The coulombic efficiency of other samples keeps steadily more than 93%. As for samples electrodeposited at the voltage of 0.7 V, although the capacity fades gradually with repeated cycling, a reversible capacity of 310–340 mA h g^{-1} is maintained for more than 50 cycles, which suggests that the electrodeposition process could provide improved electronic conductivity among the active materials and at the interface between them and the current collector. The porous structure in the Sn-based films shown in Figs. 1 and 2 could also provide more rooms to relieve the drastic volume changes during the repeated lithiathion/delithiation process, thus improving the cycleability. Moreover, it is found that the films electrodeposited at 0.7 V show the better cycle performance than those obtained at 0.5 V. Stabilized at a certain deposition voltage, films obtained with short deposition time would also produce a better cycle performance, as shown in Fig. 8. The voltage- and deposition time-dependent cycle performances might be related to the film thickness. As indicated in Table 1, higher voltage or deposition time produces a little thicker porous Sn-based film. There might be an optimized film thickness for the electrodes to deliver the better cycle performance. In this study, the optimized value of the film thickness might be around 500 nm deduced from the Table 1

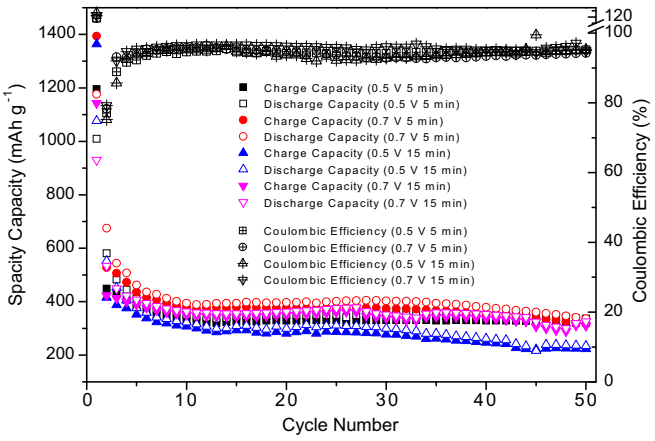

Fig. 8. Cyclic performance of the as-deposited Sn-based films at a charge-discharge rate of 100 mA g^{-1}.

and Fig. 8. The film thickness is associated with its composition as indicated in Fig. 5. Therefore, further work should be done to explore the optimized thickness ratio of SnO_2/Cu_6Sn_5 layers. In Fig. 8, it is found that the capacity of the sample obtained at 0.5 V 15 min fades rapidly after about 30 cycles, which implies a bad connection between the active materials and the current collector occurred.

The SEM micrographs of the Sn-based electrodes after 50 galvanostatical charge-discharge cycles were shown in Fig. 9. All samples in Fig. 9 show the pulverization morphologies after the repeated lithiathion/delithiation process, which is largely distinct from their as-deposited states as shown in Figs. 1 and 2. Collective particles with uniform size of about 20–50 nm are formed on the electrodes. It is also found that the pulverized active materials shown in Fig. 9a,c and d are still strongly attached on the current collector without shedding. However, as for the sample of 0.5 V 15 min shown in Fig. 9b, the active materials shed from the substrate at some local areas indicated by the arrow in the figure, which should be corresponding to its poor electrochemical performance in the cycleability (see Fig. 8). As shown in Fig. 9, the morphology of Sn-based film was dramatically changed and the original bicontinuous porous network (see Figs. 1 and 2) was not maintained by charge–discharge processes. However, the active materials were not peeled off from the current collector, which should

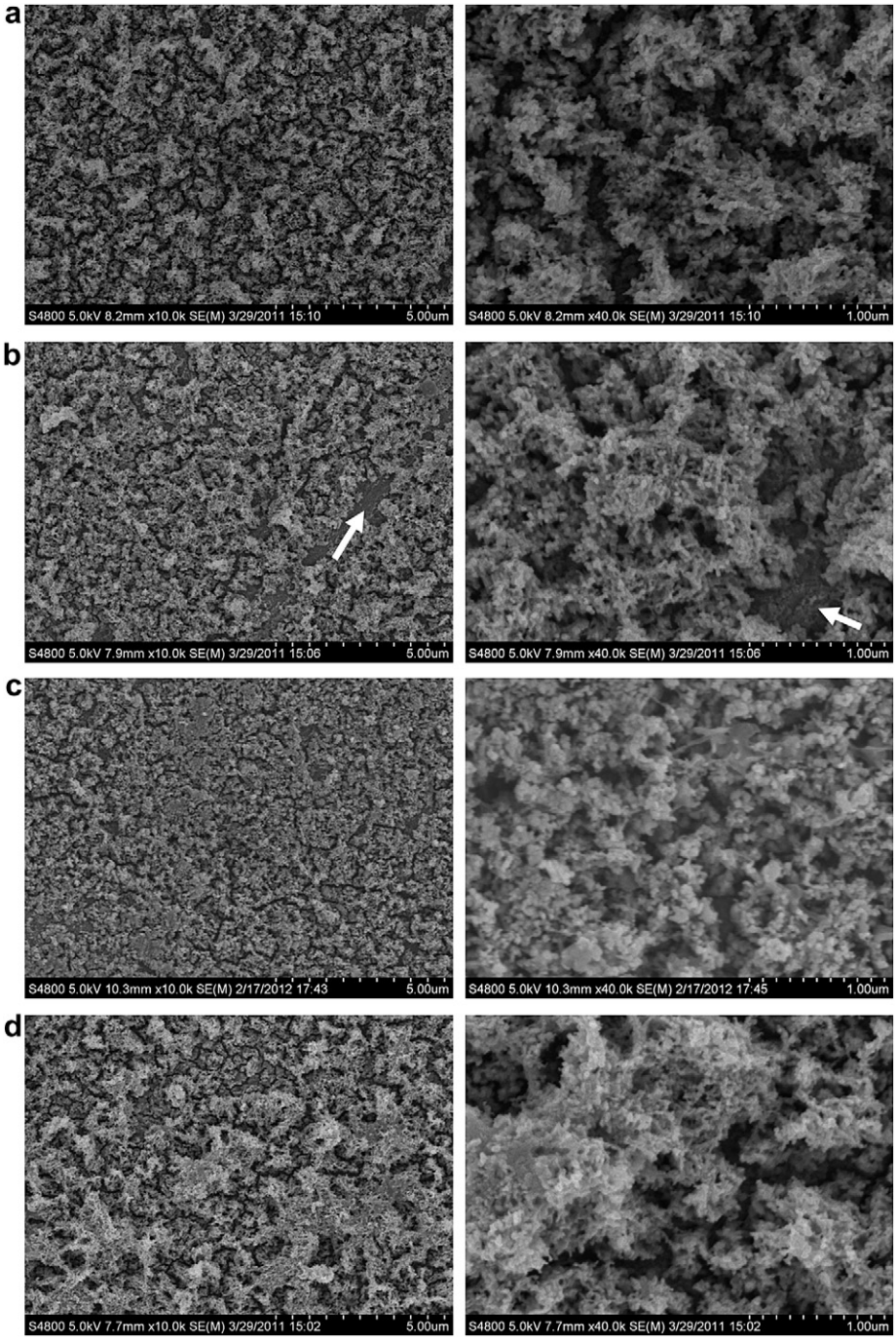

Fig. 9. SEM images of the electrodeposited Sn-based electrodes after 50 cycles at a charge-discharge rate of 100 mA g^{-1}. The electrodes were electrodeposited at 0.5 V for 5 min (a), 0.5 V for 15 min (b), 0.7 V for 5 min (c), and 0.7 V for 15 min (d), respectively.

be attributed to the porous film structure and the *in situ* formed interlocking interface between Sn and Cu as shown in Fig. 5c and d. The porous structure in the Sn-based films provides more rooms to relieve the drastic volume changes at the initial lithiathion/delithiation process. At the charge-discharge state, the inactive Cu network in the bottom layer of the electrode could interlock the active Sn and prevent the active material from peeling off the substrate.

4. Conclusion

This work provides a facile and environmental-friendly electrodeposition process to fabricate porous tin-based films from the Ethaline based electrolyte containing $SnCl_2 \cdot 2H_2O$ without any complexing agent or additive. Moreover, microstructure, composition, and electrochemical performance of the novel films were thoroughly investigated. SEM observations indicated that the initially deposited Sn grains were relatively uniform with a kind of self-assembly distribution constructing an open and bicontinuous porous network. XRD and XPS analysis revealed that these films had a double-layer structure of SnO_2/Sn–Cu alloy from the top layer to the bottom layer of the films. The porous tin-based composite films exhibited good cycle performances as anode during the repeated lithiathion/delithiation process.

Acknowledgments

The work was supported by the National Natural Science Foundation of China (51001089), the Specialized Research Fund for the Doctoral Program of Higher Education of China (20100101120026), the Research Foundation of Education Bureau of Zhejiang Province (Y200906938), the Key Science and Technology Innovation Team of Zhejiang Province under grant number 2010R50013, and the 2010 Natural Science Basic Research Open Foundation of the Key Lab of Automobile Materials, Ministry of Education, Jilin University (Grant No. 11-450060445349).

References

[1] M. Winter, J.O. Besenhard, M.E. Spahr, P. Novak, Adv. Mater. 10 (1998) 725–763.
[2] J.R. Dahn, T. Zheng, Y.H. Liu, J.S. Xue, Science 270 (1995) 590–593.
[3] Y.S. Hu, P. Adelhelm, B.M. Smarsly, S. Hore, M. Antonietti, J. Maier, Adv. Funct. Mater. 17 (2007) 1873–1878.
[4] M. Winter, J.O. Besenhard, Electrochim. Acta 45 (1999) 31–50.
[5] N. Tamura, R. Ohshita, M. Fujimoto, S. Fujitani, M. Kamino, I. Yonezu, J. Power Sources 107 (2002) 48–55.
[6] R.A. Huggins, J. Power Sources 81-82 (1999) 13–19.
[7] S.F. Yang, P.Y. Zavalij, M.S. Whittingham, Electrochem. Commun. 5 (2003) 587–590.
[8] W. Choi, J.Y. Lee, B.H. Jung, H.S. Lim, J. Power Sources 136 (2004) 154–159.
[9] C. Kim, M. Noh, M. Choi, J. Cho, B. Park, Chem. Mater. 17 (2005) 3297–3301.
[10] S.M. Paek, E. Yoo, I. Honma, Nano Lett. 9 (2009) 72–75.
[11] N.C. Li, C.R. Martin, J. Electrochem. Soc. 148 (2001) A164–A170.
[12] X.W. Lou, Y. Wang, C.L. Yuan, J.Y. Lee, L.A. Archer, Adv. Mater. 18 (2006) 2325.
[13] I.A. Courtney, J.R. Dahn, J. Electrochem. Soc. 144 (1997) 2045–2052.
[14] C.D. Gu, Y.J. Mai, J.P. Zhou, J.P. Tu, Funct. Mater. Lett. 4 (2011) 377–381.
[15] L.B. Wang, S. Kitamura, T. Sonoda, K. Obata, S. Tanase, T. Sakai, J. Electrochem. Soc. 150 (2003) A1346–A1350.
[16] L.H. Shi, H. Li, Z.X. Wang, X.J. Huang, L.Q. Chen, J. Mater. Chem. 11 (2001) 1502–1505.
[17] H. Li, L.H. Shi, W. Lu, X.J. Huang, L.Q. Chen, J. Electrochem. Soc. 148 (2001) A915–A922.
[18] N. Tamura, Y. Kato, A. Mikami, M. Kamino, S. Matsuta, S. Fujitani, J. Electrochem. Soc. 153 (2006) A1626–A1632.
[19] X.Y. Fan, Q.C. Zhuang, G.Z. Wei, L. Huang, Q.F. Dong, S.G. Sun, J. Appl. Electrochem. 39 (2009) 1323–1330.
[20] Z.J. Du, S.C. Zhang, T. Jiang, Z.M. Bai, Electrochim. Acta 55 (2010) 3537–3541.
[21] S.H. Ju, H.C. Jang, Y.C. Kang, J. Power Sources 189 (2009) 163–168.
[22] M. Armand, F. Endres, D.R. MacFarlane, H. Ohno, B. Scrosati, Nat. Mater. 8 (2009) 621–629.
[23] F. Endres, Chemphyschem 3 (2002) 144–154.
[24] S.Z. El Abedin, M. Polleth, S.A. Meiss, J. Janek, F. Endres, Green Chem. 9 (2007) 549–553.
[25] Y.S. Fung, D.R. Zhu, J. Electrochem. Soc. 149 (2002) A319–A324.
[26] M.-J. Deng, T.-I. Leong, I.W. Sun, P.-Y. Chen, J.-K. Chang, W.-T. Tsai, Electrochem. Solid-State Lett. 11 (2008) D85–D88.
[27] J.F. Huang, I.W. Sun, J. Electrochem. Soc. 150 (2003) E299–E306.
[28] A.P. Abbott, G. Capper, K.J. McKenzie, K.S. Ryder, J. Electroanal. Chem. 599 (2007) 288–294.
[29] X.H. Xu, C.L. Hussey, J. Electrochem. Soc. 140 (1993) 618–626.
[30] C.D. Gu, X.J. Xu, J.P. Tu, J. Phys. Chem. C 114 (2010) 13614–13619.
[31] A.P. Abbott, D. Boothby, G. Capper, D.L. Davies, R.K. Rasheed, J. Am. Chem. Soc. 126 (2004) 9142–9147.
[32] A.H. Whitehead, M. Polzler, B. Gollas, J. Electrochem. Soc. 157 (2010) D328–D334.
[33] A.P. Abbott, K.J. McKenzie, Phys. Chem. Chem. Phys. 8 (2006) 4265–4279.
[34] M. Mohamedi, S.J. Lee, D. Takahashi, M. Nishizawa, T. Itoh, I. Uchida, Electrochim. Acta 46 (2001) 1161–1168.
[35] X. Sun, J. Liu, Y. Li, Chem. Mater. 18 (2006) 3486–3494.
[36] D. Larcher, L.Y. Beaulieu, D.D. MacNeil, J.R. Dahn, J. Electrochem. Soc. 147 (2000) 1658–1662.